

How to GAN Event Subtraction

Anja Butter¹, Tilman Plehn¹, and Ramon Winterhalder¹

¹ Institut für Theoretische Physik, Universität Heidelberg, Germany
winterhalder@thphys.uni-heidelberg.de

June 12, 2022

Abstract

Subtracting and adding event samples are common problems in LHC simulations. We show how generative adversarial networks can produce new event samples with a phase space distribution corresponding to added or subtracted input samples. We illustrate some general features using toy samples and then show explicit examples of background and non-local collinear subtraction events in terms of unweighted 4-vector events. This event sample manipulation reflects the excellent interpolation properties of neural networks.

Content

1	Introduction	2
2	Toy example	2
2.1	Single subtraction	3
2.2	Combined subtraction and addition	6
2.3	General setup	8
3	LHC events	9
3.1	Background subtraction	9
3.2	Collinear subtraction	11
4	Outlook	12
	References	13

1 Introduction

Modern analyses of LHC data are increasingly based on a data-to-data comparison of measured and simulated events. The theoretical basis of this approach are generated samples of unweighted or weighted LHC events. To match the experimental precision such samples have to be generated beyond leading order in QCD. In modern approaches to perturbative QCD at the LHC such simulations include subtraction terms, leading to events with negative weights. Examples for such subtraction event samples are subtraction terms for fixed-order real emission [1–5], multi-jet merging including a parton shower [6, 7], on-shell subtraction [8], or the subtraction of precisely known backgrounds [9].

Generative adversarial networks or GANs [10] are neural networks which naturally lend themselves to operations on event samples, as we will show in this paper. Such generative networks have been proposed for a wide range of tasks related to LHC event simulation and are expected to lead to significant progress once they become part of the standard tool box. This includes for instance phase space integration [11, 12], event generation [13–16], detector simulations [17–23], and parton showers [24–28]. Most recently, we have shown that fully conditional GANs can be used to invert typical Monte Carlo processes at the LHC, like for instance a fast detector simulation [29]. The main feature behind these applications are the excellent interpolation properties of neural networks in a high-dimensional phase space.

In this paper, we show how GANs can perform simple operations on event samples, namely adding and subtracting existing samples. Such a network is trained to generate unweighted events with a phase space density corresponding to a sum or difference of two or more input samples. We will illustrate the idea behind a generative event sample subtraction and addition in Sec. 2. In Sec. 3 we will then subtract unweighted 4-vector events for the LHC in two examples. First we subtract the photon continuum from the complete Drell–Yan process and find the Z -pole and the known interference patterns. This can be seen as a toy example for a background subtraction at the level of parton-level event samples. Second, we combine a hard matrix element for jet radiation with collinear subtraction events. This gives us an event sample that follows the matrix element minus the subtraction term without any intermediate binning in the phase space. We show how this subtraction works even if we do not make use of the local structure of the subtraction terms, illustrating how state-of-the-art simulations in perturbative QCD might benefit from GANs.

Our applications illustrate how GANs with their excellent interpolation properties can be used to simulate subtracted events with higher precision than a statistics-limited input would (naively) suggest.

2 Toy example

The advantage of GANs learning how to subtract event samples can be seen easily from statistical uncertainties in event counts. Traditionally, we generate the two samples and combine them through some kind of histogram. If we start with $N + n$ events and subtract $N \gg n$ statistically independent events, the uncertainty on the combined events in one bin is

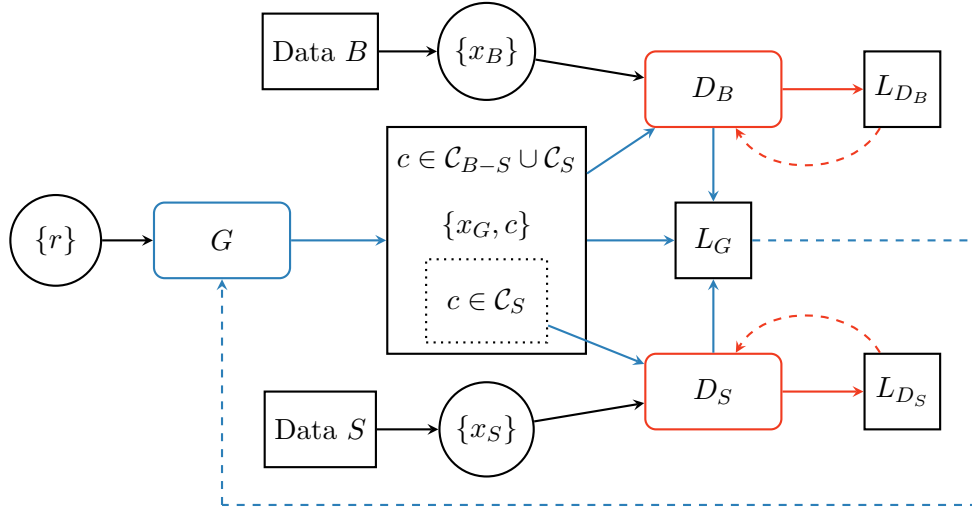


Figure 1: Structure of our subtraction GAN. The input $\{r\}$ describes a batch of random numbers and $\{x_{B,S}\}$ the true input data batches. The label c encodes the category of the generated events. Blue arrows indicate the generator training, red arrows the discriminators training.

given by

$$\Delta_n = \sqrt{\Delta_{N+n}^2 + \Delta_N^2} \approx \sqrt{2N} \gg \sqrt{n}. \quad (1)$$

In any bin-wise analysis the bin width has to be optimized. On the one hand larger bins with more events per bin minimize the relative statistical error, but on the other hand they reduce the resolution of features.

In our GAN approach we avoid defining such histograms and replace the explicit event subtraction by a subtraction of interpolated sample properties over phase space. We will first develop this approach in terms of a simple toy example and then show how it can be extended to unweighted 4-vector events as used in LHC simulations.

2.1 Single subtraction

We start with a simple 1-dimensional toy model, *i.e.* toy events which are described by a single real number x . We then define a base distribution P_B and a subtraction distribution P_S as

$$P_B(x) = \frac{1}{x} + 0.1 \quad \text{and} \quad P_S(x) = \frac{1}{x}. \quad (2)$$

The target distribution for the subtraction is then

$$P_{B-S} = 0.1. \quad (3)$$

To produce unweighted subtracted events our GAN is trained to generate the event sets $\{x_B\}$ and $\{x_S\}$ simultaneously. It thereby learns the distribution P_{B-S} using the information encoded in the two input samples.

The corresponding GAN architecture is shown in Fig. 1 and consists of a generator and two independent discriminators, one for each dataset. The generator takes random noise $\{r\}$ as input and generates samples $\{x_G, c\}$, where x_G stands for an event and c for a label. The underlying idea is to start from an event sample which follows P_B and split it into two mutually exclusive samples following P_S and P_{B-S} , with class labels \mathcal{C}_S or \mathcal{C}_{B-S} . During training we demand that the distribution over events from class \mathcal{C}_S follow P_S while the full event sample follows P_B . After normalizing all samples correctly the events with class label \mathcal{C}_{B-S} will then follow the distribution P_{B-S} .

Technically, the class label c attached to each event is a real 2-dimensional vector, such that it can be manipulated by the network. Through a SoftMax function in the final generator layer the entries of c are forced into the interval $[0, 1]$ and sum to 1. We then create a so-called one-hot encoding by mapping c to

$$c_i^{\text{one-hot}} = \begin{cases} 1 & \text{if } c_i = \max(c) \\ 0 & \text{else} \end{cases} . \quad (4)$$

This representation is two-dimensional binary and most convenient for manipulating the samples. We can use it to define the label classes via $\mathcal{C}_i = \{c \mid c_i^{\text{one-hot}} = 1\}$.

In Fig. 1 we see that for the class \mathcal{C}_S and the union of \mathcal{C}_S with \mathcal{C}_{B-S} we train the discriminators to distinguish between events from the input samples and the generated events. The training of the discriminators D_i corresponding to the two input samples $\{x_S\}$ and $\{x_B\}$ uses the standard discriminator loss function for instance in the conventions of Ref. [16]

$$L_{D_i} = \langle -\log D_i(x) \rangle_{x \sim P_T} + \langle -\log(1 - D_i(x)) \rangle_{x \sim P_G} . \quad (5)$$

We add a regularization and obtain the regularized Jensen-Shannon loss function

$$L_{D_i}^{(\text{reg})} = L_{D_i} + \lambda_{D_i} \langle (1 - D_i(x))^2 |\nabla \phi_i|^2 \rangle_{x \sim P_T} + \lambda_{D_i} \langle D_i(x)^2 |\nabla \phi_i|^2 \rangle_{x \sim P_G} , \quad (6)$$

where we define

$$\phi_i(x) = \log \frac{D_i(x)}{1 - D_i(x)} . \quad (7)$$

In parallel, we train the generator to fool the discriminators by minimizing

$$L_G = \sum_i \langle -\log D_i(x) \rangle_{x \sim P_G} . \quad (8)$$

An additional aspect in manipulating samples is that we need to keep track of the normalization or number of events in each class. To generate a clear and differentiable assignment we introduce the function

$$f(c) = e^{-\alpha(\max(c)^2 - 1)^{2\beta}} \in [0, 1] \quad \text{for} \quad 0 \leq c_i \leq 1 . \quad (9)$$

Adapting α and β we can make the gradient around the maximum steeper and push $f(0) \rightarrow 0$. In that case $f(c) \approx 1$ only if one of the entries of $c_i \approx 1$. By adding

$$L_G^{(\text{class})} = \left(1 - \frac{1}{b} \sum_{c \in \text{batch}} f(c) \right)^2 \quad (10)$$

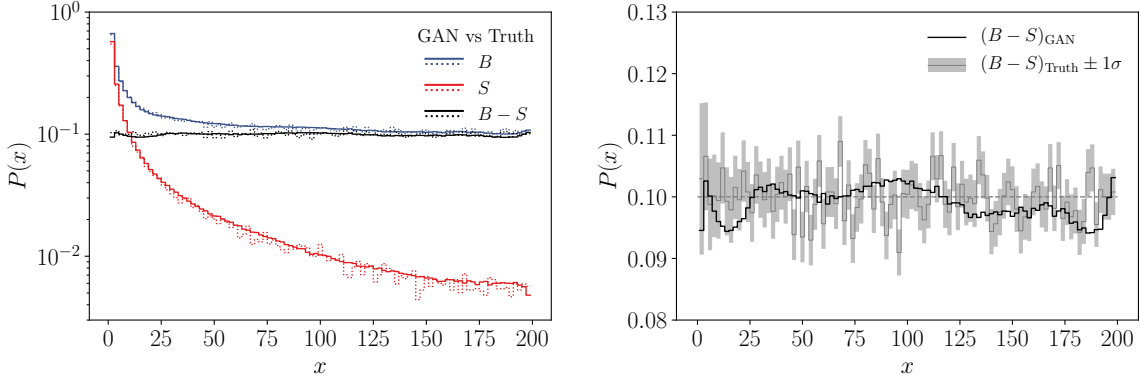


Figure 2: Left: Generated (solid) and true (dashed) events for the two input distributions and the subtracted output. Right: distribution of the subtracted events, true and generated, including the error envelope.

to the loss function we reward a clear assignment of each event to one class and generate a clear separation between classes. Finally, we use the counting function in combination with masking to fix the normalization of each sample with

$$L_{G_i}^{(\text{norm})} = \left(\frac{\sum_{c \in \mathcal{C}_i} f(c)}{\sum_{c \in \mathcal{C}_B} f(c)} - \frac{\sigma_i}{\sigma_0} \right)^2. \quad (11)$$

Adding these losses to the generator loss we get

$$L_G \rightarrow L_G^{(\text{full})} = L_G + \lambda_{\text{class}} L_G^{(\text{class})} + \lambda_{\text{norm}} L_G^{(\text{norm})}, \quad (12)$$

with properly chosen factors λ_{class} and λ_{norm} . In this paper we always use $\lambda_{\text{class}} = \lambda_{\text{norm}} = 1$. For the denominator in Eq.(11) we always choose the approximation of the number of predicted events in the base class $\mathcal{C}_B = \mathcal{C}_{B-S} \cup \mathcal{C}_S$ as reference value. The integrated rates σ_i have to be given externally. For our toy model we can compute them analytically while for an LHC application they are given by the cross section from the Monte Carlo simulation.

Our GAN uses a vector of random numbers as input. The size of the vector has to be at least the number of degrees of freedom. The discriminator and generator networks consist of 5 layers with 128 units per layer using the ELU activation function. With $\lambda_{D_i} = 5 \cdot 10^{-5}$ and a batch size of 1024 events, we run for 4000 epochs. Each epoch consists of one update of the generator and 20 updates of the discriminator. We found that the intense training of the discriminator is necessary to reach sufficiently precise results. To obtain a good separation of the classes with $f(c)$ we set $\alpha = 10$ and $\beta = 1$. Finally, we choose a learning rate of $3 \cdot 10^{-4}$ for generator and discriminator and a large decay of the learning rate of $2 \cdot 10^{-2}$ for the discriminator which stabilizes the training. The decay for the generator is slightly smaller with $5 \cdot 10^{-3}$. Our training datasets consist of 10^5 samples for each dataset $\{x_S\}$ and $\{x_B\}$.

In the left panel of Fig. 2 we show numerical results for a single GAN subtraction. In the left panel we show the two input distributions defined in Eq.(2), as well as the true and generated subtracted distribution. The dotted lines illustrate the shape of the training dataset, while the full lines show the generated distribution using $5 \cdot 10^6$ events. The former

two distributions only serve to confirm that the GAN learns the input information correctly. The generated subtracted events indeed follow the probability distribution in Eq.(3). Aside from the fact that all three distributions show excellent agreement between truth and GANned events, we see how the neural network interpolates especially in the tail of the distribution. In the right panel we zoom into the subtracted sample to compare the statistical uncertainties from the input data with the behavior of the GAN. The uncertainty is estimated from the number of events per bin in the base and subtraction histogram N_B and N_S , taking into account the corresponding normalization factors n_B and n_S . In analogy to Eq.(1) we compute it as

$$\begin{aligned}\Delta_{B-S} &= \Delta_{n_B N_B - n_S N_S} \\ &= \sqrt{\Delta_{n_B N_B}^2 + \Delta_{n_S N_S}^2} \\ &= \sqrt{n_B^2 N_B + n_S^2 N_S} .\end{aligned}\tag{13}$$

As mentioned above, we expect the GAN to deliver more stable results than we could expect from the input sample, because the GAN interpolates all input distributions. This way we avoid a bin-by-bin statistical uncertainty of the subtracted sample. Indeed, our subtracted curve in the right panel of Fig. 2 lies safely within the 1σ region of the data. In addition, the GANned distribution shows systematic deviations while the truth curve oscillates as a statistical uncertainty. The only exception are the phase space boundaries.

2.2 Combined subtraction and addition

To show how our approach could be generalized to subtracting and adding any number of event samples we can extend our single subtraction toy model by a third sample to be added to the difference described in Eq.(3). We now consider three samples corresponding to the 1-dimensional distributions

$$P_B(x) = \frac{1}{x} + 0.1 \quad P_S(x) = \frac{1}{x} \quad P_A(x) = \frac{m}{\pi} \frac{\gamma}{\gamma^2 + (x - x_0)^2} .\tag{14}$$

As a third input we add the Breit-Wigner distribution P_A , so our target distribution becomes

$$\begin{aligned}P_{B-S+A} &= \frac{m}{\pi} \frac{\gamma}{\gamma^2 + (x - x_0)^2} + 0.1 \\ &= \frac{5}{\pi} \frac{10}{100 + (x - 90)^2} + 0.1 ,\end{aligned}\tag{15}$$

	\mathcal{C}_{B-S}	\mathcal{C}_S	\mathcal{C}_A
Data B	1	1	0
Data S	0	1	0
Data A	0	0	1
$B - S + A$	1	0	1

Table 1: Category assignment for a combined addition and subtraction of three samples.

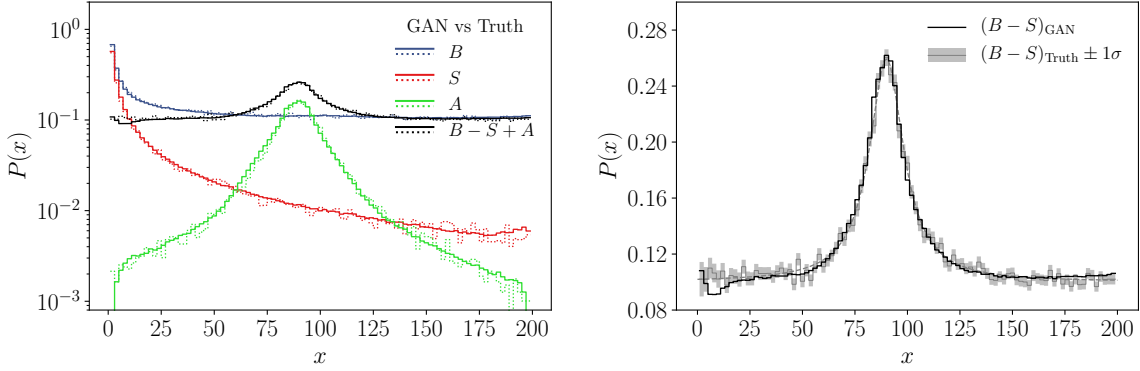


Figure 3: Left: Generated (solid) and true (dotted) events for the three input distributions and the combined output. Right: distribution of the combined events, true and generated, including the error envelope.

for the values $m = 5$, $\gamma = 10$, and $x_0 = 90$. We now sample $\{x_B\}$, $\{x_S\}$ and $\{x_A\}$ individually from the input distributions and want to learn the probability distribution P_{B-S+A} . The approach is the same as described before, but for three classes as shown in Tab. 1 and a three-dimensional class vector. Treating the subtraction exactly as before we obtain our target distribution P_{B-S+A} by adding the event with class \mathcal{C}_A .

Compared to the sample subtraction introduced before, adding samples is obviously not a big challenge. In principle, we could just add the unweighted event samples in the correct proportion, learn the phase space structure with a GAN, and then generate any number of events very efficiently. The reason why we discuss this aspect here is that it shows how our subtraction GAN can be generalized easily.

In Fig. 3 we show the numerical results of subtracting one distribution $\{x_S\}$ from the base distribution $\{x_B\}$ and adding a second distribution $\{x_A\}$ with a distinct feature. As before, this combination is learned from the three input distributions without binning the corresponding phase space. The hyper-parameters are slightly modified with respect to the simple subtraction model. The networks now consist of 7 layers with 128 units which we train for 1000 epochs with 4 iterations. We fix the relative weight of the gradient penalty to $\lambda_{D_i} = 5 \cdot 10^{-5}$. The separation of the three classes is efficient for $\alpha = 5$ and $\beta = 1$. Finally, we set the learning rate to $8 \cdot 10^{-4}$ and its decay to $2 \cdot 10^{-2}$ for generator and discriminator. The remaining parameters are the same as for the pure subtraction case. In the left panel of Fig. 3 we confirm that the GAN indeed learns the three input structures correctly and interpolates each of them smoothly. We also see that the generated events follow the combination $B-S+A$ with its flat tails and the central Breit–Wigner shape. As for the pure subtraction in Fig. 2 we also compare the statistical fluctuation of the binned input data with the behavior of the GANned events. The GAN extracts the additional Breit–Wigner feature with high precision, but, as always, some systematic deviations arise in the tails of the distribution.

classification vector c . The base class is then defined as

$$\mathcal{C} = \bigcup_{i=0}^M C_i. \quad (16)$$

In this case the network has to learn all $M + N + 1$ input distributions through individual discriminators D_B , D_{S_i} , and D_{A_j} with $i \leq M$ and $j \leq N$. The rough structure of the network is given in Fig. 4. The training of the generator follows directly from the description above. While we do not benchmark this extended setup in this paper, we expect it to be useful when a set of subtraction terms accounts for different features, and splitting them improves their simulation properties.

3 LHC events

After showing how it is possible to GAN-subtract 1-dimensional event samples from each other we have to show how such a tool can be applied in LHC physics. In this case the (unweighted) events are 4-momenta of external particles. We ignore all information on the particle identification, except for its mass, which allows us to reduce external 4-momenta to external 3-momenta [16, 29]. Because the input events might have been object to detector effects we do not assume energy-momentum conservation for the entire event. This means that the network has to learn the 4-dimensional energy-momentum conservation and this subtraction of simple LHC events is inherently multi-dimensional. We will present two simple examples for LHC event subtraction, the separation of on-shell photon and Z contributions to the Drell-Yan process and the subtraction of collinear gluon radiation in Z +jet production.

3.1 Background subtraction

Our first example for event subtraction at the LHC is the Drell-Yan process, which receives contributions with distinct phase space features from the photon and from the Z -boson, as seen in Fig. 5. The specific question in our setup is if we can subtract a background-like photon continuum contribution from the full process and generate events only for the Z -exchange combined with the interference term,

$$\begin{aligned} B : & \quad pp \rightarrow e^+ e^- \\ S : & \quad pp \rightarrow \gamma \rightarrow e^+ e^- . \end{aligned} \quad (17)$$

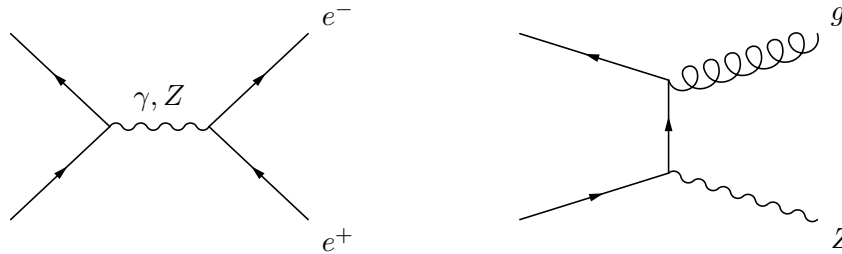


Figure 5: Sample Feynman diagrams for the background subtraction (left) and collinear subtraction (right) applications.

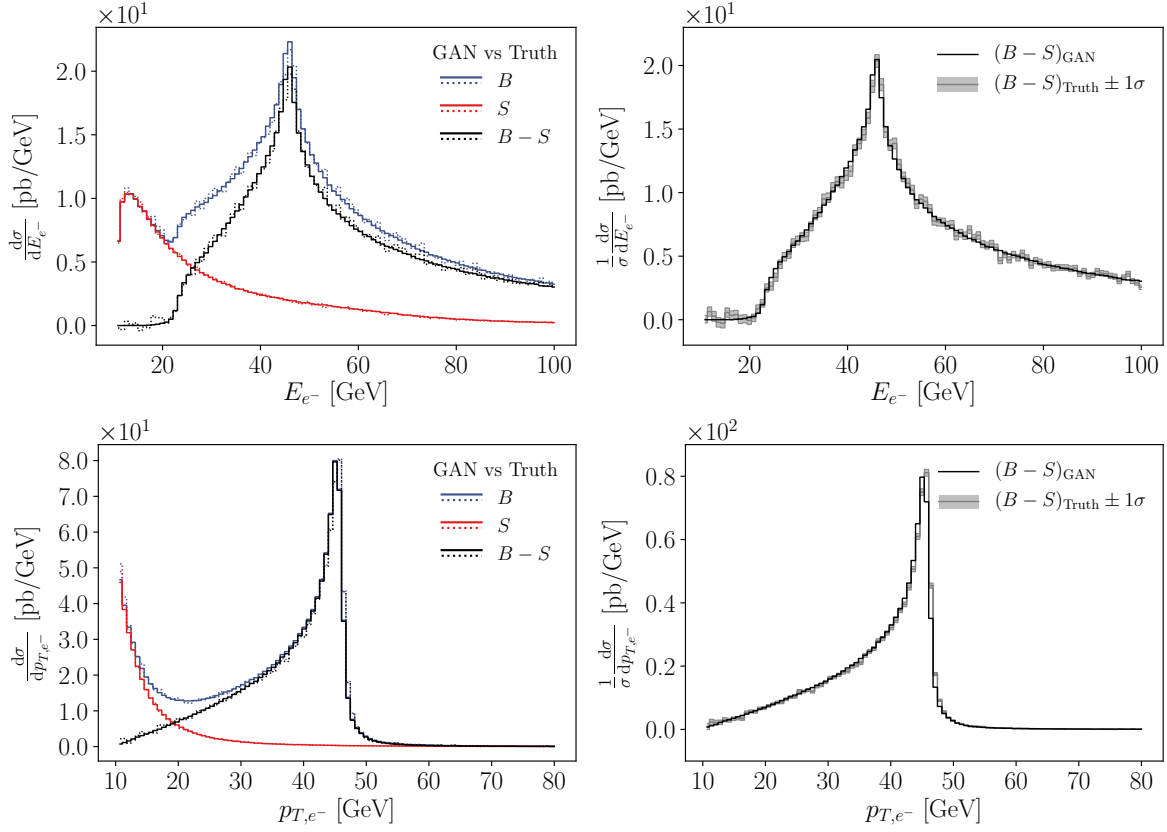


Figure 6: Left: Generated (solid) and true (dashed) e^+e^- events at the LHC for the two input distributions and the subtracted output. Right: distribution of the subtracted events, true and generated, including the error envelope.

We generate 1M events with MADGRAPH5 [30] for an LHC energy of 13 TeV, applying minimal cuts on the outgoing electrons. We require a minimal p_T of 10 GeV, a maximal rapidity of 2.5 for each electron, and a minimal angular separation of 0.4. We do not apply a detector simulation at this stage, because our focus is on comparing the generated and true distributions, and we have shown that detector simulations can be included trivially in our GAN setup [16, 29].

Aside from the increased dimension of the phase space the subtraction GAN has exactly the same structure as the toy example of Sec. 2. The hyper-parameters have to be adjusted to the increased dimensionality of the phase space. We use a 16-dimensional latent space. The discriminator and generator networks consist of 8 layers with 80 and 160 units per layer, respectively. In this high-dimensional case we use the LeakyRelu activation function. Further, we choose $\lambda_{D_i} = 10^{-5}$ and a batch size of 1024 events and train for 1000 epochs. Each epoch consists of 5 iterations in which the discriminator gets updated twice as much as the generator. For a proper separation of the classes with $f(c)$ we set $\alpha = 5$ and $\beta = 1$. Finally, we choose a large decay of the learning rate of 10^{-2} which stabilizes the training and pick a learning rate at the beginning of 10^{-3} . Our training datasets consist of 10^5 samples for each dataset $\{x_B\}$ and $\{x_S\}$.

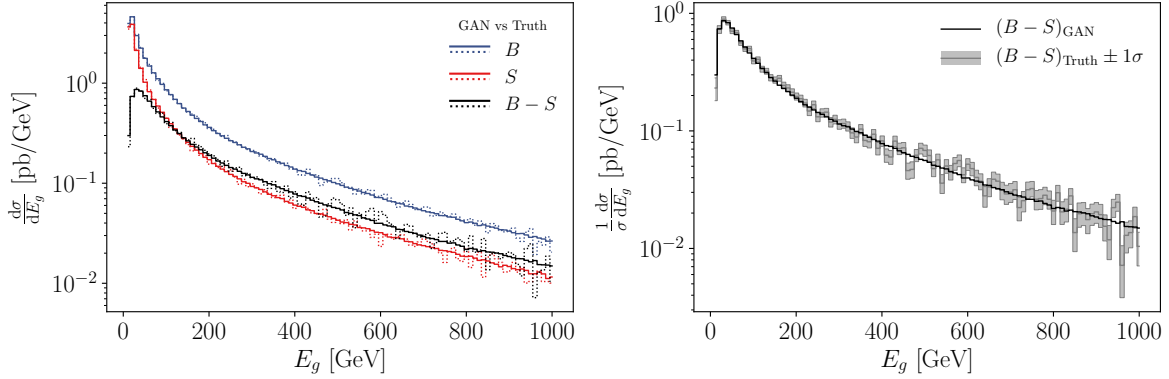


Figure 7: Left: Generated (solid) and true (dashed) Zg events at the LHC for the two input distributions and the subtracted output. Right: distribution of the subtracted events, true and generated, including the error envelope.

In Fig. 6 we show the performance of the LHC event subtraction for two example distributions. First, we clearly see the Z -mass peak in the lepton energy of the full sample, compared with the feature-less photon continuum in the subtraction sample. The subtracted curve is expected to describe the Z -contribution and the interference. It smoothly approaches zero for small lepton energies, where the interference is negligible. Above that we see the Jacobian peak from the on-shell decay, and for larger energies a small interference term enhancing the high-energy tail. In the (usual) right panel we show the subtracted curve including the statistical uncertainties from the input samples. As the second observable we show the transverse momentum of the electron. Here the Z -pole appears as a softened endpoint at $m_Z/2$. The photon continuum dominates the combined distribution for small transverse momenta. Indeed, the GAN-subtracted on-shell and interference contribution is localized around the endpoint, with a minor shift in the resolution at the edge.

3.2 Collinear subtraction

The second example for event subtraction at the LHC is collinear radiation off the initial state, for instance

$$\begin{aligned} B : & \quad pp \rightarrow Zg \quad (\text{matrix element}) \\ S : & \quad pp \rightarrow Zg \quad (\text{collinear approximation}) \end{aligned} \tag{18}$$

We generate 1M events for the hard process with SHERPA [31], where the Z -boson decays to electrons. For the network we combine the electron and positron momenta to a 4-momentum of the Z -boson, so we obtain a Breit–Wigner distribution with $m_{ee} = 66 \dots 116$ GeV instead of an on-shell condition. We then subtract the corresponding Catani-Seymour dipoles [1] for the gluon radiation off each of the incoming quarks, based on 1M events each. The corresponding Feynman diagram is shown in the right panel of Fig. 5. To avoid the soft divergence we require $E_g > 5$ GeV, a smaller cutoff would be possible but increase the training time.

The problem with this specific process is that the Catani-Seymour dipoles describe the full matrix element over a huge part of phase space [32] and the combination of hard matrix

element and dipoles is typically tiny and negative. The sign of the combination is not a problem, because we can always learn $S - B$ instead of $B - S$. Similarly, mixed signs in the S or B contributions can be accommodated by the combined subtraction and addition described in Sec. 2.2. However, the one thing a GAN cannot generate is events for which the probability distribution is compatible with zero everywhere. In this case the GAN would either over-fit statistical fluctuations or become unstable. This is why in our toy application we shift the Catani-Seymour dipole by a constant such that the cancellation of the divergent matrix element still works, but the combined result integrated over phase-space remains finite.

Note that the kinematics of our subtraction terms are not the same as in fixed-order calculations, instead it is similar to the mapping in the modified subtraction method MC@NLO [33]. In this case the global efficiency of event generators at NLO accuracy is dominated by the efficiency of computing the subtracted real-emission corrections, which presents a major challenge for event simulation at the HL-LHC [34,35].

We show the results from the collinear subtraction in Fig. 7. The GAN perfectly reconstructs the cancellation in the energy spectrum of the emitted gluon. The left panel shows the distribution of the real (B) and dipole (S) contributions to the process and their difference ($B - S$). With the logarithmic axis we see that the GAN smoothly interpolates over the entire energy range. Even in the high energy region, which suffers from low statistics, the GAN nicely matches the truth distributions. In the low energy regime, the generated distributions reproduce the phase space boundary. In the right panel we show the subtracted curve as always including the error envelope of the input.

4 Outlook

We have shown how to generate events representing the difference between two input distributions with a GAN. As a toy example we used events representing a 1-dimensional probability distribution. Because the GAN interpolates the input while learning the difference between the two distributions, it circumvents the statistical limitations of large cancellations. We have found that the GAN-subtracted events lead to a very stable phase space coverage.

For a slightly more realistic setup we have GANned background subtraction and collinear dipole subtraction for Drell–Yan production at the LHC. In the first case the network learned on-shell final state momenta to subtract the photon-induced continuum from the full e^+e^- production; in the second case we combined the hard matrix element with modified Catani-Seymour dipoles for gluon emission into a stable finite prediction of the real emission process. We are aware of the fact that our toy examples are not more than an illustration of what a subtraction GAN can achieve. However, we have shown how to use a GAN to manipulate event samples avoiding binning (at least in particle physics) and we hope that some of the people who do LHC event simulations for a living will find this technique useful.

Acknowledgments

We would like to thank Stefan Höche for extremely useful discussions and for helping us out with specially made SHERPA events on really short notice. In addition, we would like

to thank Olivier Mattelaer for his incredibly friendly help with MADGRAPH5. Finally, we would like to thank Kirill Melnikov for inspiring this project and Gregor Kasieczka for his continuous input on machine learning and GANs. RW acknowledges support by the IMPRS for *Precision Tests of Fundamental Symmetries*. The research of AB and TP is supported by the Deutsche Forschungsgemeinschaft (DFG, German Research Foundation) under grant 396021762 — TRR 257 *Particle Physics Phenomenology after the Higgs Discovery*.

References

- [1] S. Catani and M. H. Seymour, Phys. Lett. **B378** (1996) 287, arXiv:hep-ph/9602277 [hep-ph].
- [2] S. Höche, S. Liebschner, and F. Siegert, Eur. Phys. J. **C79** (2019) 9, 728, arXiv:1807.04348 [hep-ph].
- [3] A. Gehrmann-De Ridder, T. Gehrmann, and E. W. N. Glover, JHEP **09** (2005) 056, arXiv:hep-ph/0505111 [hep-ph].
- [4] R. Frederix, T. Gehrmann, and N. Greiner, JHEP **09** (2008) 122, arXiv:0808.2128 [hep-ph].
- [5] J. Currie, E. W. N. Glover, and S. Wells, JHEP **04** (2013) 066, arXiv:1301.4693 [hep-ph].
- [6] S. Catani, F. Krauss, R. Kuhn, and B. R. Webber, JHEP **11** (2001) 063, arXiv:hep-ph/0109231 [hep-ph].
- [7] M. L. Mangano, M. Moretti, F. Piccinini, R. Pittau, and A. D. Polosa, JHEP **07** (2003) 001, arXiv:hep-ph/0206293 [hep-ph].
- [8] D. Gonçalves-Netto, D. López-Val, K. Mawatari, T. Plehn, and I. Wigmore, Phys. Rev. **D87** (2013) 1, 014002, arXiv:1211.0286 [hep-ph].
- [9] T. Plehn and M. Takeuchi, J. Phys. **G38** (2011) 095006, arXiv:1104.4087 [hep-ph].
- [10] I. J. Goodfellow, J. Pouget-Abadie, M. Mirza, B. Xu, D. Warde-Farley, S. Ozair, A. Courville, and Y. Bengio, arXiv:1406.2661 [stat.ML].
- [11] M. D. Klimek and M. Perelstein, arXiv:1810.11509 [hep-ph].
- [12] J. Bendavid, arXiv:1707.00028 [hep-ph].
- [13] S. Otten *et al.*, arXiv:1901.00875 [hep-ph].
- [14] B. Hashemi, N. Amin, K. Datta, D. Olivito, and M. Pierini, arXiv:1901.05282 [hep-ex].
- [15] R. Di Sipio, M. Faucci Giannelli, S. Ketabchi Haghighat, and S. Palazzo, JHEP **08** (2020) 110, arXiv:1903.02433 [hep-ex].
- [16] A. Butter, T. Plehn, and R. Winterhalder, SciPost Phys. **7** (2019) 075, arXiv:1907.03764 [hep-ph].

- [17] M. Paganini, L. de Oliveira, and B. Nachman, Phys. Rev. Lett. **120** (2018) 4, 042003, arXiv:1705.02355 [hep-ex].
- [18] M. Paganini, L. de Oliveira, and B. Nachman, Phys. Rev. **D97** (2018) 1, 014021, arXiv:1712.10321 [hep-ex].
- [19] P. Musella and F. Pandolfi, Comput. Softw. Big Sci. **2** (2018) 1, 8, arXiv:1805.00850 [hep-ex].
- [20] M. Erdmann, L. Geiger, J. Glombitza, and D. Schmidt, Comput. Softw. Big Sci. **2** (2018) 1, 4, arXiv:1802.03325 [astro-ph.IM].
- [21] M. Erdmann, J. Glombitza, and T. Quast, Comput. Softw. Big Sci. **3** (2019) 4, arXiv:1807.01954 [physics.ins-det].
- [22] ATLAS Collaboration, Tech. Rep. ATL-SOFT-PUB-2018-001, CERN, Geneva, Jul, 2018.
- [23] ATLAS Collaboration, A. Ghosh, Tech. Rep. ATL-SOFT-PUB-2019-007, CERN, Geneva, Jun, 2019.
- [24] E. Bothmann and L. Debbio, JHEP **01** (2019) 033, arXiv:1808.07802 [hep-ph].
- [25] L. de Oliveira, M. Paganini, and B. Nachman, Comput. Softw. Big Sci. **1** (2017) 1, 4, arXiv:1701.05927 [stat.ML].
- [26] J. W. Monk, JHEP **12** (2018) 021, arXiv:1807.03685 [hep-ph].
- [27] A. Andreassen, I. Feige, C. Frye, and M. D. Schwartz, Eur. Phys. J. **C79** (2019) 2, 102, arXiv:1804.09720 [hep-ph].
- [28] S. Carrazza and F. A. Dreyer, Eur. Phys. J. **C79** (2019) 11, 979, arXiv:1909.01359 [hep-ph].
- [29] M. Bellagente, A. Butter, G. Kasieczka, T. Plehn, and R. Winterhalder, arXiv:1912.00477 [hep-ph].
- [30] J. Alwall *et al.*, JHEP **07** (2014) 079, arXiv:1405.0301 [hep-ph].
- [31] E. Bothmann *et al.*, SciPost Phys. **7** (2019) 3, 034, arXiv:1905.09127 [hep-ph].
- [32] J. Campbell, J. Huston, and F. Krauss, *The Black Book of Quantum Chromodynamics*. Oxford University Press, 2017.
- [33] S. Frixione and B. R. Webber, JHEP **06** (2002) 029, arXiv:hep-ph/0204244 [hep-ph].
- [34] HEP Software Foundation, J. Albrecht *et al.*, Comput. Softw. Big Sci. **3** (2019) 1, 7, arXiv:1712.06982 [physics.comp-ph].
- [35] A. Buckley, arXiv:1908.00167 [hep-ph].